Eur. Phys. J. C (2023) 83:70
https://doi.org/10.1140/epjc/s10052-023-11177-8

THE EUROPEAN PHYSICAL JOURNAL C

Regular Article - Theoretical Physics

P_{cc}^N states in a unitarized coupled-channel approach

Chao-Wei Shen[1,a], **Yong-hui Lin**[2,b], **Ulf-G. Meißner**[2,1,3,c]

[1] Institute for Advanced Simulation, Institut für Kernphysik and Jülich Center for Hadron Physics, Forschungszentrum Jülich, 52425 Jülich, Germany
[2] Helmholtz-Institut für Strahlen- und Kernphysik and Bethe Center for Theoretical Physics, Universität Bonn, 53115 Bonn, Germany
[3] Tbilisi State University, 0186 Tbilisi, Georgia

Received: 29 August 2022 / Accepted: 30 December 2022 / Published online: 24 January 2023

Abstract Starting from an effective Lagrangian with heavy quark spin symmetry embedded, the coupled-channel dynamics of the doubly charmed systems $D^{(*)}\Sigma_c^{(*)}$ is investigated. The potential underlying our investigation includes t-channel pseudoscalar and vector meson exchanges. A series of S-wave bound states with isospin $I = 1/2$ is found by applying the first iterated solution of the N/D method: one state with binding energy 23 MeV in the $5/2^-$ $D^*\Sigma_c^*$ channel, three states with binding energy 26, 30 and 7 MeV (relative to the thresholds from low to high, respectively) in the $3/2^-$ $D\Sigma_c^*$-$D^*\Sigma_c$-$D^*\Sigma_c^*$ system and three states with binding energy 32, 8 and 16 MeV in the $1/2^-$ $D\Sigma_c$-$D^*\Sigma_c$-$D^*\Sigma_c^*$ system. Those P_{cc}^N states serve as the open-charm partners of the hidden charm pentaquarks P_ψ^N observed by the LHCb Collaboration.

1 Introduction

Searches of exotic hadrons, whose valence quark composition is beyond the conventional picture where mesons and baryons are composed of a pair of quark-antiquark ($q\bar{q}$) and three quarks (qqq), respectively, have become an important project for most of the collider facilities especially after the experimental observations of tetraquark and pentaquark candidates [1–7]. In 2015, the LHCb Collaboration announced the first evidence of two hidden-charm pentaquark-like states $P_\psi^N(4380)$ and $P_\psi^N(4450)$ in the $J/\psi p$ invariant mass spectrum measured from the decay process $\Lambda_b^0 \to J/\psi K^- p$ [6]. In 2019, the mass spectrum of P_ψ^N pentaquarks was updated to three states, that is, $P_\psi^N(4312)$, $P_\psi^N(4440)$ and $P_\psi^N(4457)$ by the LHCb Collaboration [8]. In 2020, a new hidden-charm pentaquark state with strangeness, namely $P_{\psi s}^\Lambda(4459)$, was observed in the $J/\psi\Lambda$ invariant mass distribution from the $\Xi_b^- \to J/\psi\Lambda K^-$ decay [9]. And very recently, another hidden-charm pentaquark with strangeness, $P_{\psi s}^\Lambda(4338)$, was announced by the LHCb Collaboration [10]. It is observed in the invariant mass spectrum of $J/\psi\Lambda$ in the decay $B^- \to J/\psi\Lambda\bar{p}$. In the last decade, the LHCb Collaboration has found many surprises in exotic hadron spectroscopy. One can expect that the richness of the exotic spectrum will continue to increase in the foreseeable future.

The theoretical investigations on the exotic spectroscopy date back to the birth of the quark model in 1964. The existence of pentaquark states was first pointed out by Gell-Mann in his famous paper on the quark model [11]. From the point of view of modern physics, neither the multiquark states that made up of more than three valence quarks such as tentraquarks ($qq\bar{q}\bar{q}$) and pentaquarks ($qqqq\bar{q}$), nor the hybrid states that have both valence quarks and gluons or the glueballs that are composed of pure valence gluons are forbidden by Quantum Chromodynamics (QCD), which is the fundamental theory of the strong interactions. Before the first experimental evidence of P_ψ^N, these pentaquark states have been predicted by the theoretical work based on the phenomenological coupled-channel approach in 2010 [12,13]. In that work, one $\bar{D}\Sigma_c$ and one $\bar{D}^*\Sigma_c$ bound state were found around 4 GeV, which can be related to the observed $P_\psi^N(4312)$ and $P_\psi^N(4440)$ (or $P_\psi^N(4457)$) states, respectively. In particular, the newly reported $P_{\psi s}^\Lambda(4459)$ and $P_{\psi s}^\Lambda(4338)$ states are also compatible with the predicted $\bar{D}^*\Xi_c$ and $\bar{D}\Xi_c$ bound states, respectively. Such impressive consistence between the experimental observations and the

[a] e-mail: c.shen@fz-juelich.de
[b] e-mail: yonghui@hiskp.uni-bonn.de (corresponding author)
[c] e-mail: meissner@hiskp.uni-bonn.de

theoretical predictions on the pentaquark spectrum around 4 GeV is a strong indication for the molecular nature of those pentaquark-like states. The hadronic molecule picture has become a much discussed approach to explain the nature of the exotic candidates, as seen by the many theoretical studies of exotic hadron spectroscopy during the last decades, see the recent reviews in Refs. [14–18].

In Ref. [19], the authors claim that the near-threshold structures exist generally in two heavy hadron systems as long as the interaction between them is attractive. Hundreds of hadronic molecules are proposed in the heavy-heavy [20–23] and heavy-antiheavy sectors [24]. And very recently, several five-flavored bound states are predicted in the $B^{(*)}\Xi_c^{(\prime)}$ system [25]. Among these exotic baryons, the doubly-charmed pentaquarks are straightforward extensions of the P_ψ^N states, whose quark content can be written as $ccqq\bar{q}$ ($q = u, d$). In this work, we explore the mass spectrum of the doubly-charmed pentaquark-like states around 4 GeV. Some earlier investigations on this system are given in Refs. [20–23]. Reference [21] constructed the contact, one-pion-exchange, and two-pion-exchange potentials for the coupled-channel $D^{(*)}\Sigma_c^{(*)}$ system within the framework of a chiral effective field theory and found the S-wave bound states by solving the nonrelativistic Schrödinger equation. Reference [23] updated the configuration in Ref. [21] by introducing the S-D mixing effect within the one-boson-exchange (OBE) model assisted with heavy quark spin symmetry (HQSS) and Refs. [20,22] only studied the single channel case where the S-D mixing effect was also considered in Ref. [20]. All those three works give a similar mass spectrum for the doubly-charmed pentaquark candidates, that is, one $1/2^-$ $D\Sigma_c$, one $3/2^-$ $D\Sigma_c^*$, two $D^*\Sigma_c$ with spin-parity $1/2^-$ and $3/2^-$, and three $D^*\Sigma_c^*$ bound states with spin-parity $1/2^-$, $3/2^-$ and $5/2^-$. All those doubly-charmed bound states have isospin $I = 1/2$ and the binding energies vary from several MeV to tens of MeV.

In the present work, both pseudoscalar (π, η) and vector (ρ, ω) meson exchanges are considered by means of an effective Lagrangians that is constrained by the HQSS together with the chiral symmetry for the pseudoscalar meson part and the hidden local symmetry for the vector meson part. The bound states and resonances are found as poles of the coupled-channel scattering amplitudes given by a unitarized Bethe-Salpeter equation (BSE) in the on-shell factorization approach. Further, the first iterated solution of the N/D method is employed to avoid the unphysical left-hand-cut problem in the on-shell factorized BSE [26,27].

This work is organized as follows. In Sect. 2, we present the theoretical framework of our calculation. The numerical results for the $D\Sigma_c$, $D\Sigma_c^*$, $D^*\Sigma_c$ and $D^*\Sigma_c^*$ coupled-channel dynamics and relevant discussions are presented in Sect. 3. Finally, a brief summary is given in Sect. 4. Some technicalities are relegated to the Appendices.

Table 1 S-wave channels in the $D\Sigma_c$-$D\Sigma_c^*$-$D^*\Sigma_c$-$D^*\Sigma_c^*$ coupled-channel system. The quantum numbers are given in the spectroscopic form $^{2S+1}L_J$

Channel	$J^P = 1/2^-$	$3/2^-$	$5/2^-$
$D\Sigma_c$	$^2S_{1/2}$	–	–
$D\Sigma_c^*$	–	$^4S_{3/2}$	–
$D^*\Sigma_c$	$^2S_{1/2}$	$^4S_{3/2}$	–
$D^*\Sigma_c^*$	$^2S_{1/2}$	$^4S_{3/2}$	$^6S_{5/2}$

2 Formalism

Before going to the details of our theoretical calculations, we briefly count the number of channels in the coupled-channel $D^{(*)}\Sigma_c^{(*)}$ system included in our work. It should be noticed that we only consider S-wave scattering with isospin $I = 1/2$ throughout the present work. The quantum numbers of the various $D^{(*)}\Sigma_c^{(*)}$ channels are listed in Table 1. It shows that we have three channels ($D\Sigma_c$, $D^*\Sigma_c$ and $D^*\Sigma_c^*$) for spin-parity $J^P = 1/2^-$, three channels ($D\Sigma_c^*$, $D^*\Sigma_c$ and $D^*\Sigma_c^*$) for $J^P = 3/2^-$, and one channel ($D^*\Sigma_c^*$) for $J^P = 5/2^-$.

2.1 Effective Lagrangians and the on-shell factorization approach of the Bethe–Salpeter equation

Chiral perturbation theory (ChPT) developed in the 1980 s [28–30] has achieved great success in describing low-energy experiments of the strong interaction, especially the $\pi\pi$ and πN scattering [31]. A variety of ChPT variants were proposed to solve various specific strong-interaction systems. Among them, the heavy baryon and heavy meson chiral perturbation theory are designed to describe the interactions between two hadrons containing one or more heavy quarks [32–35], see Ref. [18] for a recent review. Similar to the ChPT language, the interactions between two heavy hadrons are constructed from light pseudoscalar exchange, the Goldstone bosons from the spontaneous breaking of chiral symmetry. The interactions between heavy hadrons and light vector mesons are built by using the hidden local symmetry approach [36–38]. All the relevant effective Lagrangians used here are given as [24,39]

$$\begin{aligned}
\mathcal{L}_1 &= ig\langle H_b^{(Q)}\mathcal{A}_{ba}^{\mu}\gamma_\mu\gamma_5\bar{H}_a^{(Q)}\rangle,\\
\mathcal{L}_2 &= -i\beta\langle H_b^{(Q)}v^\mu\rho_{\mu,ba}\bar{H}_a^{(Q)}\rangle\\
&\quad + i\lambda\langle H_b^{(Q)}\sigma^{\mu\nu}(\partial_\mu\rho_\nu - \partial_\nu\rho_\mu)_{ba}\bar{H}_a^{(Q)}\rangle,\\
\mathcal{L}_S &= -\frac{3}{2}g_1 v_\kappa\epsilon^{\mu\nu\lambda\kappa}\bar{S}_{\mu,ab}^{(Q)}\mathcal{A}_{\nu,bc}S_{\lambda,ca}^{(Q)} - i\beta_S\bar{S}_{\mu,ab}^{(Q)}v^\alpha\rho_{\alpha,bc}\\
&\quad\times S_{ca}^{(Q)\mu} + \lambda_S\bar{S}_{\mu,ab}^{(Q)}(\partial^\mu\rho^\nu - \partial^\nu\rho^\mu)_{bc}S_{\nu,ca}^{(Q)},
\end{aligned} \tag{1}$$

where the Lorentz indices are given by the greek letters $\mu, \nu, \ldots$, the SU(3) flavor indices are denoted by latin sym-

bols $a, b, \ldots$ and $\langle \cdots \rangle$ is the Dirac trace. The summation over repeated indices is implicit. The explicit formulae for all vertices in our t-channel potentials are then obtained by expanding the above Lagrangians. Note that we neglect the heavy quark spin symmetry breaking effects induced by the finite charm quark mass, which is roughly estimated as $\mathcal{O}(\Lambda_{\rm QCD}/m_c) \approx 15\%$ variation in the contact constant interaction prescription, see e.g., Ref. [40]. The expansion of the underlying Lagrangians and the definitions of the involved field operators are displayed in Appendix A.

The scattering amplitude T is unitarized through the Bethe-Salpeter equation, namely

$$T = V + VGT, \tag{2}$$

where V is the scattering kernel that is expressed in terms of the t-channel one-boson-exchange transitions between two channels and G is the two-meson loop function. In the coupled-channel case, T is a $n \times n$ matrix (n denotes the number of the coupled channels) and G becomes a n-dimension diagonal matrix with all the elastic loop functions g_i as its elements (i is the channel index). Working with the on-shell factorization approach, the integral equation (2) is reduced to an algebraic equation and one can solve the amplitude T with

$$T = (1 - VG)^{-1} V. \tag{3}$$

Unitarity and analyticity of T are guaranteed in the on-shell factorization prescription in most cases [41–43]. And it has been applied commonly into various hadron systems to study the low-energy strong interaction dynamics in them, see e.g., [15,18,44–51] (and references therein). It should also be mentioned that in some cases where the unphysical left-hand cuts (usually come from the partial-wave projection of V) are not far away from the energy regions of interest, the unitarity and analyticity of T become problematic due to the existence of such unphysical cuts, see e.g., Refs. [27,52] for more details.

For the two-meson Green's function g_i, we adopt dimensional regularization to arrive at

$$\begin{aligned} g_i &= i \int \frac{d^4q}{(2\pi)^4} \frac{1}{(p-q)^2 - M_B^{i2} + i\varepsilon} \frac{1}{q^2 - M_P^{i2} + i\varepsilon} \\ &= \frac{1}{16\pi^2} \Bigg\{ a(\mu) + \ln \frac{M_B^{i2}}{\mu^2} + \frac{M_P^{i2} - M_B^{i2} + s}{2s} \ln \frac{M_P^{i2}}{M_B^{i2}} \\ &\quad + \frac{\bar{q}_i}{\sqrt{s}} \Big[\ln(s - M_B^{i2} + M_P^{i2} + 2\bar{q}_i\sqrt{s}) \\ &\quad + \ln(s + M_B^{i2} - M_P^{i2} + 2\bar{q}_i\sqrt{s}) \\ &\quad - \ln(-s - M_B^{i2} + M_P^{i2} + 2\bar{q}_i\sqrt{s}) \\ &\quad - \ln(-s + M_B^{i2} - M_P^{i2} + 2\bar{q}_i\sqrt{s}) \Big] \Bigg\}, \end{aligned} \tag{4}$$

where $s = p^2$ and

$$\bar{q}_i = \sqrt{\frac{(s - (M_B^i + M_P^i)^2)(s - (M_B^i - M_P^i)^2)}{4s}}.$$

M_B^i, M_P^i denote the baryon and meson masses in the channel i, and $a(\mu)$ is the scale-dependent subtract constant. Note that $\mathrm{Im}(\bar{q}) \geq 0$ indicates that Eq. (4) gives the loop function in the physical sheet, denoted as g_i^I. The loop function in the unphysical sheet, denoted as g_i^{II}, is then expressed as

$$g_i^{II}(s) = g_i^I + 2i\rho_i(s), \tag{5}$$

with $\rho_i(s) = \bar{q}_i/(8\pi\sqrt{s})$. Another strategy commonly adopted to calculate the loop function G is to introduce a phenomenological form factor, such as the Gaussian regulator, in the integral, that is,

$$g_i = \int \frac{q^2 dq}{4\pi^2} \frac{\omega_B^i + \omega_P^i}{\omega_B^i \omega_P^i} \frac{e^{-2q^2/\Lambda^2}}{s - (\omega_B^i + \omega_P^i)^2 + i\varepsilon}, \tag{6}$$

where ω_B^i and ω_P^i are the on-shell energies for the baryon and meson in ith channel, respectively. In this work, we take the convention of Eq. (4), where $a(\mu)$ is estimated by matching g_i of Eq. (4) to the one of Eq. (6) at ith threshold with the empirical values of cutoff Λ, i.e., around 1 GeV.

2.2 First iterated solution of the N/D method

As mentioned above, the existence of the left-hand cuts (LHC) could invalidate the on-shell factorization formula of Eq. (3) in some cases. Unfortunately, this indeed happens in the $D^{(*)}\Sigma_c^{(*)}$ systems of interest. In this subsection, we briefly introduce the N/D method that can be used to treat those unphysical LHC properly [26,27,43,53,54].

In the N/D method, the unitarized scattering amplitude T is constructed through the dispersion relations and it has the general form

$$T(s) = D(s)^{-1} N(s), \tag{7}$$

where the numerator $N(s)$ and denominator $D(s)$ contain the analytic information of the left- and right-hand cuts, respectively. The general expressions of $N(s)$ and $D(s)$ for the S-wave are given by

$$\begin{aligned} D(s) &= \sum_{m=0}^{n-1} a_m s^m + \frac{(s-s_0)^n}{\pi} \int_{s_{\rm thr}}^{\infty} ds' \frac{\rho(s') N(s')}{(s'-s)(s'-s_0)^n}, \\ N(s) &= \sum_{m=0}^{n-1} b_m s^m + \frac{(s-s_0)^n}{\pi} \int_{-\infty}^{s_{\rm left}} ds' \frac{\mathrm{Im}T(s') D(s')}{(s'-s)(s'-s_0)^n}, \end{aligned} \tag{8}$$

where the polynomials $\sum_m a_m s^m$ and $\sum_m b_m s^m$ denote the subtraction terms with a_m and b_m the corresponding subtrac-

tion constants. s_0 is the subtraction point and n is the number of subtractions that is required to ensure the convergence of the dispersion integrals. Note that the so-called Castiliejo–Dalitz–Dyson (CDD) poles [55] are dropped here. The difficulty caused by the unphysical LHC will be overcome if one solves exactly the N/D integral equations Eq. (8). An approximative strategy called the first-iterated solution of the N/D method that was proposed in Refs. [26,27] is utilized in our work. It states that we approximate the numerator $N(s)$ as the tree-level potential $V(s)$ and then the denominator $D(s)$ can be expressed as

$$D_{ij}(s) = \gamma_{0ij} + \gamma_{1ij}(s - s^j_{\rm thr}) + \frac{1}{2}\gamma_{2ij}(s - s^j_{\rm thr})^2 + \frac{(s - s^j_{\rm thr})s^2}{\pi}\int_{s^j_{\rm thr}}^{\infty} ds' \frac{V_{ij}(s')\rho_j(s')}{(s' - s^j_{\rm thr})(s' - s)s'^2}, \quad (9)$$

where i and j are the channel indices. The subtraction point s_0 is set to be $s^j_{\rm thr}$, the jth threshold, and $n = 3$. Three subtraction constants γ_{0ij}, γ_{1ij} and γ_{2ij} are determined by matching $D_{ij}(s)$ of Eq. (9) and $\delta_{ij} - V_{ij}(s)G_j$ around the threshold $s^j_{\rm thr}$ for each i and j, specifically. We fit $D_{ij}(s)$ of Eq. (9) to $\delta_{ij} - V_{ij}(s)G_j$ in the small energy region from the threshold $s^j_{\rm thr}$ to 100 MeV above it. It is worth mentioning that G_j in the matching procedure is the loop function in the physical sheet. Consequently, the scattering amplitude T of the physical sheet is calculated with the D function constructed in Eq. (9). Further, T in the unphysical sheets are defined as [27],

$$T^{II}(s) = \frac{1}{[T^I(s)]^{-1} - 2i\rho}, \quad (10)$$

where ρ denotes the diagonal matrix diag$\{N_i\rho_i(s)\}$ with $N_i = 0$ and 1 representing the physical and unphysical sheets for the ith channel. The uncertainty stemming from the ambiguity of the choice of the matching energy region will be discussed when we present our numerical results. For further discussions on the validity of the first-iterated solution of the N/D method, we refer to Refs. [26,27].

3 Results and discussions

First, we focus on the case of $J^P = 5/2^-$ and explain the necessity of treating the LHC in the partial-wave projected potentials by using the N/D method. The S-wave potential for the $5/2^-$-$D^*\Sigma_c^*$ system is given in terms of the t-channel ρ-, ω-, π- and η-exchange diagrams. The numerical potential $V_{D^*\Sigma_c^*\to D^*\Sigma_c^*}$ is presented in Fig. 1. One can clearly see that the S-wave projection for each boson exchange produces one LHC located below the $D^*\Sigma_c^*$ threshold. Among them, the LHC corresponding to the π exchange is quite close to the threshold and that from the vector meson exchange is stronger.

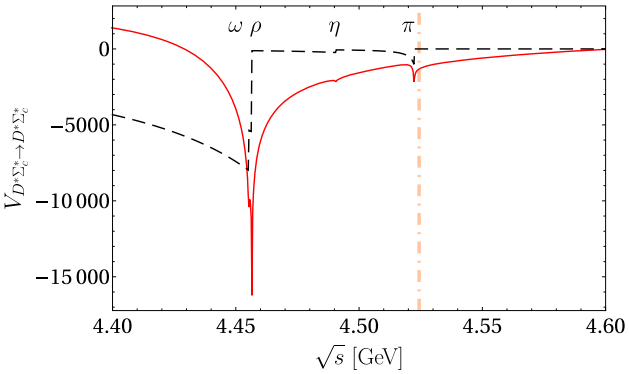

Fig. 1 S-wave potential for $D^*\Sigma_c^* \to D^*\Sigma_c^*$ with $(I, J) = (1/2, 5/2)$ (real part: solid curve, imaginary part: dashed curve). The corresponding threshold is represented by the orange dash-dotted line. The left-hand cuts from left to right are generated by the ω, ρ, η and π exchange, respectively

The $(1 - VG)$ term in Eq. (3) and D in Eq. (9) of the physical Riemann sheet RS(+) with the cutoff $\Lambda = 0.7$ GeV for the S-wave $5/2^-$-$D^*\Sigma_c^*$ system are shown in the left and right panel of Fig. 2, respectively. The pole position of scattering amplitude T in the single channel case is represented by the zeros of $(1 - VG)$ in the on-shell factorization BSE approach or equivalently the zeros of the D function in the N/D method.

It can be seen from Fig. 2 that there no pole appears in the function $1 - VG$ and one pole located below the threshold at the real axis can be found in the D function which is related to a $D^*\Sigma_c^*$ bound state with binding energy $E_B = 53$ MeV. However, all the previous works imply the existence of an S-wave $D^*\Sigma_c^*$ bound state with $J^P = 5/2^-$ [20–22]. To be more specific, Ref. [21] claimed an S-wave $D^*\Sigma_c^*$ state with binding energy being around 20 MeV in the non-relativistic one- and two-pion exchange potentials. Reference [22] found a bound state from the non-relativistic ρ- and ω-exchange interactions with the binding energy varying from 2 to 40 MeV. And a 40-to-90 MeV binding energy was produced by Ref. [20] with the OBE model. The S-wave $D^*\Sigma_c^*$ state with $E_B = 53$ MeV obtained from the N/D method is consistent with these previous non-relativistic investigations.

Next, we turn to the $D\Sigma_c^*$-$D^*\Sigma_c$-$D^*\Sigma_c^*$ coupled-channel system with $(I, J) = (1/2, 3/2)$. The V matrix is presented in Fig. 3. Similar to the $J^P = 5/2^-$ single channel case, all the meson-exchange potentials contain the left-hand cuts after implementing the partial-wave projection except the one-pion-exchange parts in $V_{D\Sigma_c^*\to D^*\Sigma_c}$ and $V_{D\Sigma_c^*\to D^*\Sigma_c^*}$. In particular, the left-hand cuts from the η-exchange interaction in $V_{D\Sigma_c^*\to D^*\Sigma_c^*}$ and the π-exchanges in the elastic potentials $V_{D^*\Sigma_c\to D^*\Sigma_c}$ and $V_{D^*\Sigma_c^*\to D^*\Sigma_c^*}$ are quite close to

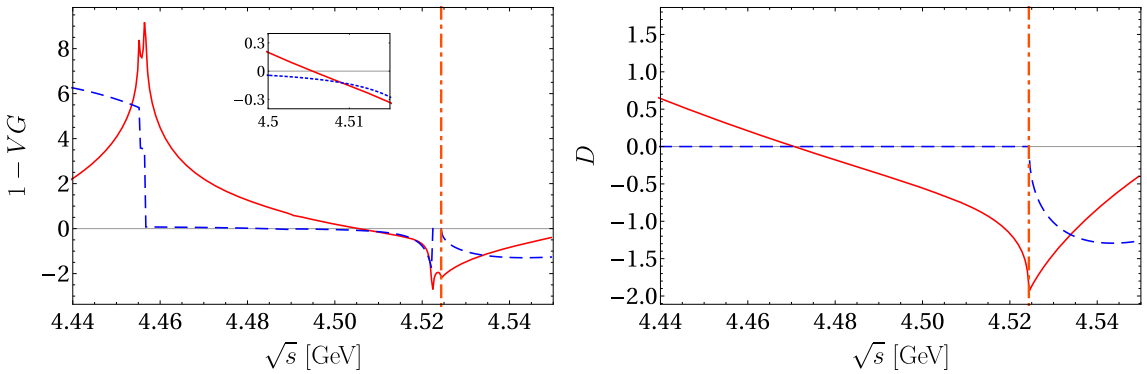

Fig. 2 $(1 - VG)$ (left panel) and D (right panel) in the physical sheet for the S-wave $D^*\Sigma_c^*$ system with $(I, J) = (1/2, 5/2)$ (real part: solid curve, imaginary part: dashed curve). The cutoff is $\Lambda = 0.7$ GeV. The corresponding threshold is represented by the orange dash-dotted line

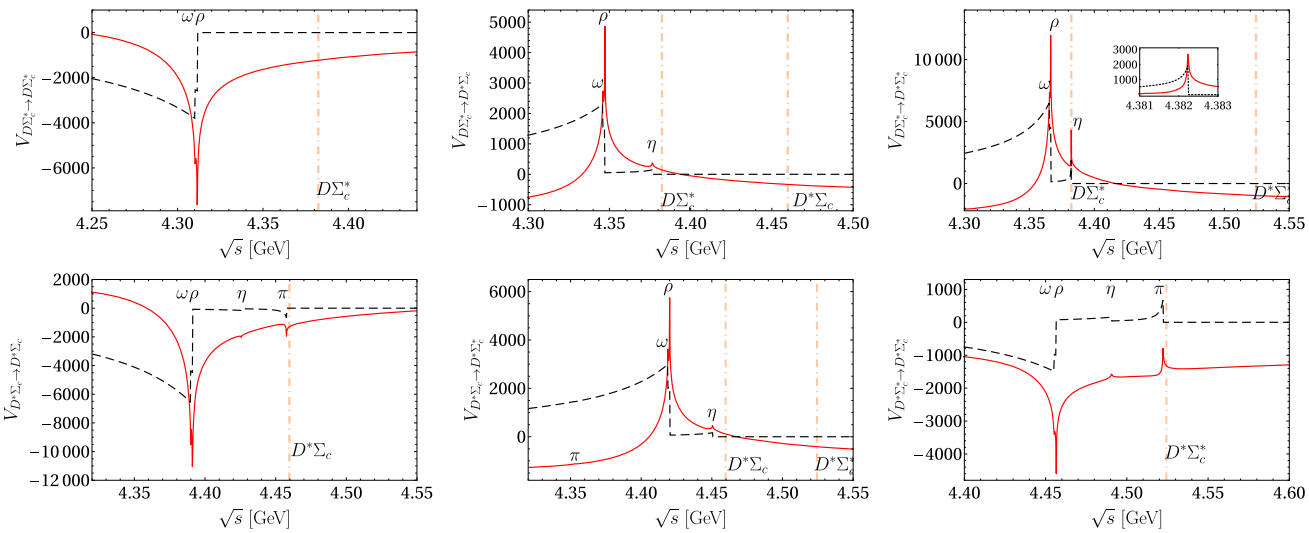

Fig. 3 V matrix for the S-wave $D\Sigma_c^*$-$D^*\Sigma_c$-$D^*\Sigma_c^*$ coupled-channel system with $(I, J) = (1/2, 3/2)$ (real part: solid curve, imaginary part: dashed curve). The corresponding threshold is represented by the orange dash-dotted line

and below the lower thresholds. For these cases, the dispersion relations used in N/D method are still valid since no LHC goes above the RHC. However, the effects left in the unitarized scattering amplitude T by those near-threshold LHC are difficult to remove completely. To do so as much as possible, we shift the energy region, where the subtraction constants in the D functions of Eq. (9) are fitted to functions $(1-VG)$ in Eq. (3) a bit above the corresponding thresholds. In practice, the D_{ij} functions are fitted to $\delta_{ij} - V_{ij}G_j$ in the energy range starting from 10 MeV above the jth threshold up to 100 MeV above it. Then the pole positions are found to be zeros of determinants of D for the physical sheet and $([T^I]^{-1} - 2i\rho)$ for the unphysical sheets. The pole trajectory in the unphysical sheet RS$(--+)$ for the $3/2^-$ $D\Sigma_c^*$-$D^*\Sigma_c$-$D^*\Sigma_c^*$ coupled-channel system is shown in Fig. 4. When Λ is less than 0.5 GeV, no $D^*\Sigma_c^*$ bound state with $J^P = 3/2^-$ is found. The cutoff range from 0.6 to 0.8 GeV is then chosen to give the full mass spectrum in this work. Note that the cutoff Λ constitutes a hard momentum scale which suppresses the contribution of the two-body constituents in the given channels at short distances $\sim 1/\Lambda$. There is no universal criterion for the determination of a such cut-off and for the choice of the regulator functions, but as a general rule the value of Λ should be much larger than the typical momentum in the bound state, given by $\sqrt{2\mu\epsilon}$ (~ 0.1 GeV for the present case) [15]. Further, it should not be too large since we have neglected all other degrees of freedom that would play a role at short distances.

The calculations for the $D\Sigma_c$-$D^*\Sigma_c$-$D^*\Sigma_c^*$ coupled channels with $(I, J) = (1/2, 1/2)$ can be done along similar lines. The V matrix for $(I, J) = (1/2, 1/2)$ is given in Fig. 5.

Finally, all the obtained pole positions are collected in the Table 2. Similar to other previous works [21–23], one $D\Sigma_c$ bound state with $J^P = 1/2^-$, one $D\Sigma_c^*$ bound state with $J^P = 3/2^-$ and one $D^*\Sigma_c^*$ bound state with $J^P = 5/2^-$ are found. These three states are located at the physical real axis and below the threshold of the lowest channel in the corresponding systems, thus they are bound states. Two res-

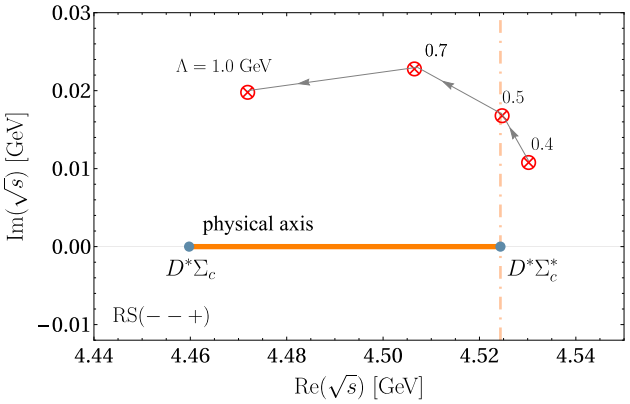

Fig. 4 The pole trajectory on the sheet RS(− − +) of the S-wave $D\Sigma_c^*$-$D^*\Sigma_c$-$D^*\Sigma_c^*$ coupled-channel system with $(I, J) = (1/2, 3/2)$. The cutoff Λ is varied from 0.4 to 1.0 GeV. The highest threshold is represented by the orange dash-dotted line. The pole positions are denoted as the red crosses. The sheet RS(− − +) intersects with the physical region at the thick orange line that connects the $D^*\Sigma_c$ and $D^*\Sigma_c^*$ thresholds

onances located at the complex plane of the unphysical sheets RS(− + +) and RS(− − +) are found in both $1/2^-$ and $3/2^-$ coupled channels, which are related to the $D^*\Sigma_c$ and $D^*\Sigma^*$ bound states with corresponding spin-parities obtained in the single-channel investigations by Ref. [22]. The sensitivities of various pole positions to the cutoff are different, the most sensitive case is the $5/2^-$ $D^*\Sigma_c^*$ pole, whose binding energy varies from 23 MeV to 110 MeV as the cutoff changed from 0.6 GeV to 0.8 GeV, and the least sensitive one is the $1/2^-$ $D^*\Sigma_c$ pole, whose binding energy varies from 8 MeV to 18 MeV. Noted that all the widths of resonances depend on the Λ only mildly and thus the averaged values are listed.

We plot the full mass spectrum together with the uncertainty caused by the cutoff Λ in Fig. 6. For completeness, one should also consider the estimation of the uncertainties caused by those effective coupling constants. As discussed in Appendix A, however, most couplings are estimated model-dependently by means of the vector meson dominance approach or using the quark model. Then it is difficult to implement a reliable estimation for the errors of these coupling constants. Here, as an illustration, we only show the effect of coupling g which is fixed as -0.59 ± 0.07 through the decay of $D^* \to D\pi$ [56]. It leads to the uncertainty of 53 ± 5 MeV for the binding energy of the $(1/2, 5/2)$-$D^*\Sigma_c^*$ state when $\Lambda = 0.7$ GeV, which is a marginal effect compared to the cutoff variation. Moreover, the theoretical error from the ambiguity of the matching energy region that needed

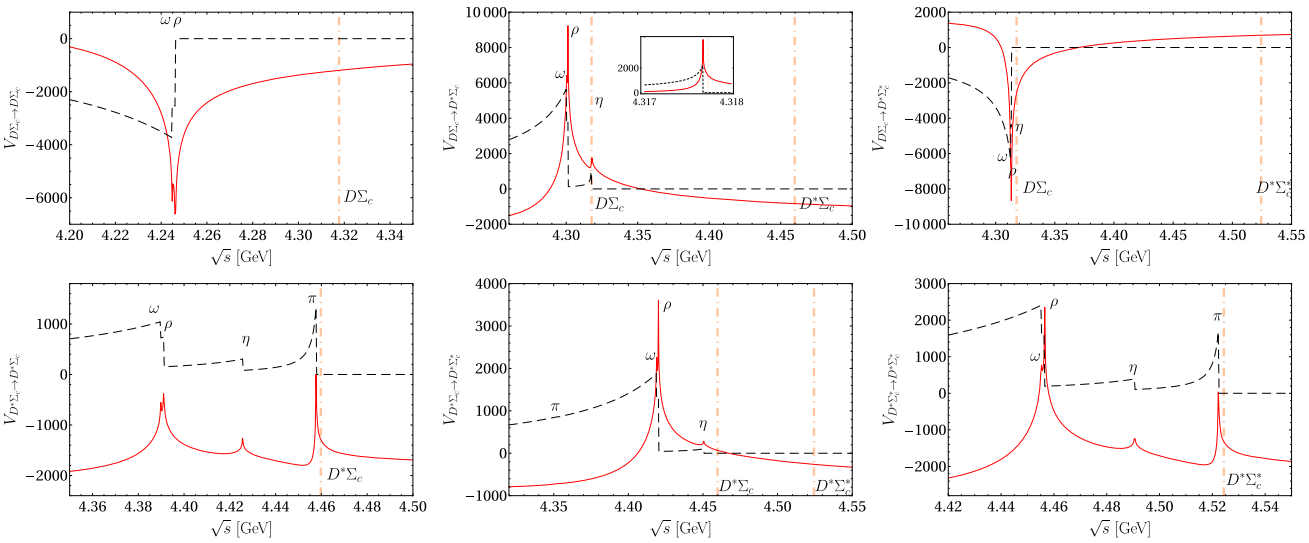

Fig. 5 V matrix for the S-wave $D\Sigma_c$-$D^*\Sigma_c$-$D^*\Sigma_c^*$ coupled-channel system with $(I, J) = (1/2, 1/2)$. For notations, see Fig. 3

Table 2 Pole positions obtained from the $5/2^-$ $D^*\Sigma_c^*$, $3/2^-$ $D\Sigma_c^*$-$D^*\Sigma_c$-$D^*\Sigma_c^*$ and $1/2^-$ $D\Sigma_c$-$D^*\Sigma_c$-$D^*\Sigma_c^*$ systems. The cutoff Λ is varied in the range of (0.6, 0.8) GeV. All the pole positions are given in units of MeV and the corresponding thresholds are listed in the brackets in the first column

Channel	$1/2^-$	$3/2^-$	$5/2^-$
$D\Sigma_c(4318)$	(4223, 4286)	–	–
$D\Sigma_c^*(4382)$	–	(4295, 4356)	–
$D^*\Sigma_c(4460)$	$(4442, 4452) + 20i$	$(4367, 4440) + 1i$	–
$D^*\Sigma_c^*(4524)$	$(4490, 4508) + 10i$	$(4496, 4518) + 20i$	(4415, 4501)

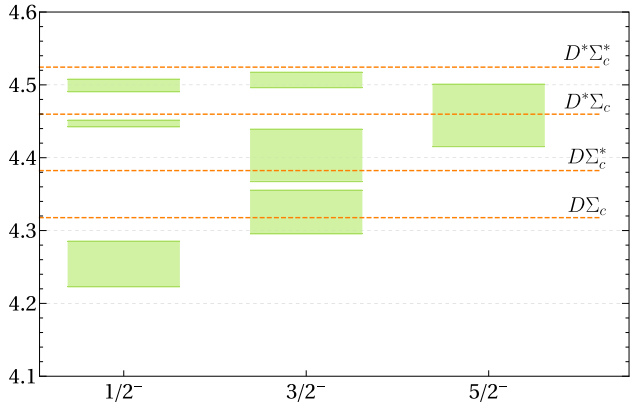

Fig. 6 Mass spectrum of the S-wave $D\Sigma_c^*$-$D^*\Sigma_c$-$D^*\Sigma_c^*$ coupled-channel dynamics with $(I, J) = (1/2, 3/2)$, S-wave $D\Sigma_c$-$D^*\Sigma_c$-$D^*\Sigma_c^*$ system with $(I, J) = (1/2, 1/2)$ and S-wave $D^*\Sigma_c^*$ channel with $(I, J) = (1/2, 5/2)$, respectively. The cutoff Λ is varied from 0.6 GeV to 0.8 GeV. For the resonances, only the real parts of their pole positions are presented

for the determination of the subtraction constants in Eq. (9) is also estimated. The variation of this matching range from (10, 100) MeV above threshold to (30, 100) MeV induces an additional uncertainty of 10–20% on the binding energies of the various poles. It should be mentioned that the elimination of those near-threshold left-hand cuts in this work by employing the first-iterated N/D method is rather qualitative and not a rigorous treatment. To investigate the mass spectrum in the $D^{(*)}\Sigma_c^{(*)}$ coupled-channel systems more quantitatively and precisely, a more rigorous and elegant treatment to the unphysical left-hand cuts is required. Nevertheless, there is no doubt that the open-charm partners of those LHCb pentaquark states do exist and are located close to the corresponding $D^{(*)}\Sigma_c^{(*)}$ thresholds. One can expect those P_{cc}^N states around 4 GeV will be observed experimentally in the near future.

4 Summary

Recently, several pentaquark-like states, P_ψ^N close to $\bar{D}^{(*)}\Sigma_c^{(*)}$ thresholds and $P_{\psi s}^\Lambda$ close to the $\bar{D}^{(*)}\Xi_c^{(*)}$, were reported by the LHCb Collaboration. All these pentaquark states are suggested to be the hadronic molecule candidates composed of the corresponding meson–baryon pairs close to the pertinent thresholds, see e.g., Refs. [14–18] (and references therein). The extensions of the mass spectrum of pentaquark states assisted by the heavy quark spin symmetry and flavor symmetry are expected straightforwardly. In this work, we explore the possible open-charm partners of P_ψ^N states by investigating the S-wave $D^{(*)}\Sigma_c^{(*)}$ coupled-channel dynamics. Unitarized scattering amplitudes are constructed by means of the first-iterated N/D method. The open-charm partners of P_ψ^N are predicted as follows: for $I(J^P) = 1/2(1/2^-)$, one $D\Sigma_c$ bound state with $E_B = 32$ MeV, one $D^*\Sigma_c$ state with $E_B = 8$ MeV and one $D^*\Sigma_c^*$ state with $E_B = 16$ MeV; for $I(J^P) = 1/2(3/2^-)$, one $D\Sigma_c^*$ bound state with $E_B = 26$ MeV, one $D^*\Sigma_c$ state with $E_B = 20$ MeV and one $D^*\Sigma_c^*$ state with $E_B = 7$ MeV; for $I(J^P) = 1/2(5/2^-)$, one $D^*\Sigma_c^*$ state with $E_B = 23$ MeV. Further investigations are required to solidify these results.

Acknowledgements We thank Meng-Lin Du and Yu-Fei Wang for useful discussions and comments. This work is supported in part by the Deutsche Forschungsgemeinschaft (DFG) and the National Natural Science Foundation of China (NSFC) through the funds provided to the Sino-German Collaborative Research Center "Symmetries and the Emergence of Structure in QCD" (NSFC Grant no. 12070131001, DFG Project-ID 196253076—TRR 110). The work of UGM was supported in part by The Chinese Academy of Sciences (CAS) President's International Fellowship Initiative (PIFI) (Grant no. 2018DM0034) and by the VolkswagenStiftung (Grant no. 93562).

Data Availability Statement This manuscript has no associated data or the data will not be deposited. [Authors' comment: This article is dedicated to build the mass spectrum of pentaquark-like states in the open-charm sector near 4.5 GeV from the theoretical perspective. No experimental data is involved. And all obtained theoretical descriptions are displayed as figures and tables in our article.]

Funded by SCOAP[3]. SCOAP[3] supports the goals of the International Year of Basic Sciences for Sustainable Development.

Appendix A: Effective Lagrangians and exchange potentials

After expanding the effective Lagrangians in Eq. (1), one has

$$\begin{aligned}
\mathcal{L}_1 &= \frac{-\sqrt{2}g}{F_\pi}[-i\epsilon_{\tau\alpha\mu\nu}v^\alpha P_b^{*(Q)\mu}\partial^\nu \Pi_{ba} P_a^{*(Q)\tau\dagger} \\
&\quad + P_b^{*(Q)\mu}\partial_\mu \Pi_{ba} P_a^{(Q)\dagger} + P_b^{(Q)}\partial^\nu \Pi_{ba} P_{a\nu}^{*(Q)\dagger}], \\
\mathcal{L}_2 &= \sqrt{2}\beta g_V (P_b^{*(Q)\mu} v^\nu V_{\nu,ba} P_{\mu,a}^{*(Q)\dagger} \\
&\quad - P_b^{(Q)} v^\nu V_{\nu,ba} P_a^{(Q)\dagger}) - i2\sqrt{2}\lambda g_V \Big[P_b^{*(Q)\mu}(\partial_\mu V_{\nu,ba} \\
&\quad - \partial_\nu V_{\mu,ba}) P_a^{*(Q)\nu\dagger} \\
&\quad + i\epsilon_{\tau\lambda\nu\alpha} v^\alpha P_b^{(Q)} \partial^\tau V_{ba}^\lambda P_a^{*(Q)\nu\dagger}
\end{aligned}$$

$$
\begin{aligned}
&- i\epsilon_{\alpha\mu\tau\lambda} v^{\alpha} P_b^{*(Q)\mu} \partial^{\tau} V_{ba}^{\lambda} P_a^{(Q)\dagger} \Big], \\
\mathcal{L}_S = &\frac{-i3g_1}{2\sqrt{2}F_\pi} v_\kappa \epsilon^{\mu\nu\lambda\kappa} \Big[\bar{B}_{6\mu,ab}^{*(Q)} \\
&+ \frac{1}{\sqrt{3}} \bar{B}_{6,ab}^{(Q)} \gamma_5 \gamma_\mu \Big] \partial_\nu \Pi_{bc} \Big[B_{6\lambda,ca}^{*(Q)} - \frac{1}{\sqrt{3}} \gamma_\lambda \gamma_5 B_{6,ca}^{(Q)} \Big] \\
&+ \frac{\beta_S g_V}{\sqrt{2}} \Big[\bar{B}_{6\mu,ab}^{*(Q)} \\
&+ \frac{1}{\sqrt{3}} \bar{B}_{6,ab}^{(Q)} \gamma_5 (\gamma_\mu + v_\mu) \Big] v^{\alpha} V_{\alpha,bc} \Big[B_{6,ca}^{*(Q)\mu} \\
&- \frac{1}{3} (\gamma^{\mu} + v^{\mu}) \gamma_5 B_{6,ca}^{(Q)} \Big] + \frac{i\gamma_S g_V}{\sqrt{2}} \Big[\bar{B}_{6\mu,ab}^{*(Q)} \\
&+ \frac{1}{\sqrt{3}} \bar{B}_{6,ab}^{(Q)} \gamma_5 (\gamma_\mu + v_\mu) \Big] (\partial^{\mu} V^{\nu} - \partial^{\nu} V^{\mu})_{bc} \\
&\Big[B_{6\nu,ca}^{*(Q)} - \frac{1}{\sqrt{3}} (\gamma_\nu + v_\nu) \gamma_5 B_{6,ca}^{(Q)} \Big], \qquad \text{(A1)}
\end{aligned}
$$

in terms of the various field operators

$$
\begin{aligned}
P^{(*)(Q)} &= \sqrt{M} (D^{(*)0}, D^{(*)+}, D_s^{(*)+}), \\
\Pi &= \begin{pmatrix} \frac{\pi^0}{\sqrt{2}} + \frac{\eta}{\sqrt{6}} & \pi^+ & K^+ \\ \pi^- & -\frac{\pi^0}{\sqrt{2}} + \frac{\eta}{\sqrt{6}} & K^0 \\ K^- & \bar{K}^0 & -\sqrt{\frac{2}{3}}\eta \end{pmatrix}, \\
V &= \begin{pmatrix} \frac{\rho^0}{\sqrt{2}} + \frac{\omega}{\sqrt{2}} & \rho^+ & K^{*+} \\ \rho^- & -\frac{\rho^0}{\sqrt{2}} + \frac{\omega}{\sqrt{2}} & K^{*0} \\ K^{*-} & \bar{K}^{*0} & \phi \end{pmatrix}, \\
B_6^{(Q)} &= \begin{pmatrix} \Sigma_c^{++} & \frac{1}{\sqrt{2}}\Sigma_c^{+} & \frac{1}{\sqrt{2}}\Xi_c^{\prime +} \\ \frac{1}{\sqrt{2}}\Sigma_c^{+} & \Sigma_c^{0} & \frac{1}{\sqrt{2}}\Xi_c^{\prime 0} \\ \frac{1}{\sqrt{2}}\Xi_c^{\prime +} & \frac{1}{\sqrt{2}}\Xi_c^{\prime 0} & \Omega_c^{0} \end{pmatrix}, \\
B_6^{*(Q)} &= \begin{pmatrix} \Sigma_c^{*++} & \frac{1}{\sqrt{2}}\Sigma_c^{*+} & \frac{1}{\sqrt{2}}\Xi_c^{*+} \\ \frac{1}{\sqrt{2}}\Sigma_c^{*+} & \Sigma_c^{*0} & \frac{1}{\sqrt{2}}\Xi_c^{*0} \\ \frac{1}{\sqrt{2}}\Xi_c^{*+} & \frac{1}{\sqrt{2}}\Xi_c^{*0} & \Omega_c^{*0} \end{pmatrix}. \qquad \text{(A2)}
\end{aligned}
$$

The values of the coupling constants adopted in the present work are given in Table 3. The pion decay constant $F_\pi = 92.3\,\text{MeV}$ is used as in Reference [39] and $g_V = M_\rho/(\sqrt{2}F_\pi) = 5.8$ is fixed with the help of the vector meson dominance (VMD) approach [38]. g_1 is related to the coupling g_4 by heavy quark symmetry, that is, $g_1 = 2\sqrt{2}/3 g_4$ with the latter determined by the decay of $\Sigma_c^* \to \Lambda_c \pi$ [33,39]. And the signs of g_1 and g_4 are fixed using the quark model [33]. The parameter g is inferred from the decay of $D^* \to D\pi$ with its sign fixed by either QCD sum rules or the quark model, see Ref. [35] for the details of sign determination. Note that we take the sign convention for g in Ref. [57]. It is different from that in Ref. [56], which would cause a sign difference in g, while the latest absolute value we adopted is from Ref. [56]. $\beta = \sqrt{2}M_\rho/(g_V f_\rho)$ is obtained with the VMD method [56] with $f_\rho = 210\,\text{MeV}$. As for λ, it is estimated from the experimental data on the $D \to K^*$ form factor by using the effective Lagrangian method and its sign is fixed by applying the VMD approach into the $D^* D\gamma$ vertex [35]. Here we take the updated value of λ in Ref. [56]. Both magnitudes and signs of λ_S and β_S are fixed within the quark model [58]. It should be mentioned that there exist various sign conventions of these effective couplings in different papers depending on the definitions of the field operators and Lagrangians. What really matters is the sign of the potential kernel in the dynamical equations, which shows whether the considered interaction is attractive or repulsive.

Table 3 The coupling constants adopted in the calculations

g_V [38]	g_1 [39]	g [56,57]	λ_S [58]	λ [35,56]
5.8	0.94	− 0.59	− 3.31/GeV	0.56/GeV
β [56]	β_S [58]	F_π [39]		
0.9	− 1.74	0.092 GeV		

Table 4 The combined coupling factors and isospin factors for all the involved processes. It implies the first seven reactions contains the π, η, ρ and ω exchange, while the last two only have the ρ and ω exchange

Process	Exchanged particle	CF	IF
$\Sigma_c D \to \Sigma_c D^*$	π	$\frac{1}{2}$	2
$\Sigma_c D \to \Sigma_c^* D^*$			
$\Sigma_c^* D \to \Sigma_c D^*$	η	$\frac{1}{6}$	1
$\Sigma_c^* D \to \Sigma_c^* D^*$			
$\Sigma_c D^* \to \Sigma_c D^*$	ρ	$\frac{1}{2}$	2
$\Sigma_c D^* \to \Sigma_c^* D^*$			
$\Sigma_c^* D^* \to \Sigma_c^* D^*$	ω	$\frac{1}{2}$	1
$\Sigma_c D \to \Sigma_c D$	ω	$\frac{1}{2}$	1
$\Sigma_c^* D \to \Sigma_c^* D$	ρ	$\frac{1}{2}$	2

For each process, besides the pseudo-potential $\mathcal{V}$, which can be derived from the effective Lagrangians above, there also exists a combined coupling factor (CF) and an isospin factor (IF). The combined coupling factor comes from the combination of different charged particles for the same process. We collect all the involved combined coupling factors in Table 4. The isospin factors are calculated using [59]

$$
\begin{aligned}
IF(I) = &\sum_{m_1,m_2,m_3,m_4} \langle I_1 m_1 I_2 m_2 | I I_z \rangle \langle I_3 m_3 I_4 m_4 | I I_z \rangle \\
&\times \langle I_3 m_3 I_4 m_4 | M^{iso} | I_1 m_1 I_2 m_2 \rangle, \qquad \text{(A3)}
\end{aligned}
$$

with the baryon-first convention is applied. $\langle j_1 m_1 j_2 m_2 | j_3 m_3 \rangle$ represents the Clebsch-Gordan coefficient $(m_1 m_2 m_3 | j_1 j_2 j_3)$ related to the composition $\boldsymbol{j}_1 + \boldsymbol{j}_2 = \boldsymbol{j}_3$. All the isospin fac-

tors for the considered processes are also given in Table 4. Then the transition amplitude with specified quantum numbers is expressed by

$$V = -(\mathrm{CF}) \times (\mathrm{IF}) \times \mathcal{V}. \tag{A4}$$

Here the minus sign comes from the definition that ensures a negative V corresponds to an attraction interaction.

Appendix B: Partial-wave analysis

Once the potential respecting heavy quark spin symmetry is calculated, we can get the partial-wave potential in the JLS basis using [26,60]

$$\begin{aligned} T^J_{LS;L'S'}(s) &= \frac{Y^0_{L'}(\hat{\mathbf{z}})}{2J+1} \sum_{\substack{s_{1z},s_{2z},s_{3z},\\ s_{4z},m}} \int \mathrm{d}\hat{\mathbf{p}}' Y^m_L(\hat{\mathbf{p}}')^* \\ &\times (s_{1z}s_{2z}S_z|s_1s_2S)(mS_zS'_z|LSJ) \\ &\times (s_{3z}s_{4z}S'_z|s_3s_4S')(0S'_zS'_z|L'S'J)T(s) \\ &\overset{m=0}{=} \frac{\sqrt{(2L'+1)(2L+1)}}{2J+1} \sum_{\substack{s_{1z},s_{2z},\\ s_{3z},s_{4z}}} \frac{1}{2}\int_{-1}^{1} \mathrm{d}\cos\theta \\ &\times P_L(\cos\theta)(s_{1z}s_{2z}S_z|s_1s_2S)(0S_zS'_z|LSJ) \\ &\times (s_{3z}s_{4z}S'_z|s_3s_4S')(0S'_zS'_z|L'S'J)T(s). \end{aligned} \tag{B1}$$

Regarding that only the S-wave term is considered in the present work, e.g., $L = L' = 0$, we then have the following expression

$$\begin{aligned} T^J_{0S;0S'}(s) &= \frac{1}{2J+1} \sum_{\substack{s_{1z},s_{2z},\\ s_{3z},s_{4z}}} \frac{1}{2}\int_{-1}^{1} \mathrm{d}\cos\theta (s_{1z}s_{2z}S_z|s_1s_2S) \\ &\times (s_{3z}s_{4z}S_z|s_3s_4S')T(s)\,. \end{aligned} \tag{B2}$$

References

1. S.K. Choi et al. (Belle), Phys. Rev. Lett. **91**, 262001 (2003)
2. B. Aubert et al. (BaBar), Phys. Rev. Lett. **95**, 142001 (2005)
3. A. Bondar et al. (Belle), Phys. Rev. Lett. **108**, 122001 (2012)
4. M. Ablikim et al. (BESIII), Phys. Rev. Lett. **110**, 252001 (2013)
5. M. Ablikim et al. (BESIII), Phys. Rev. Lett. **111**(24), 242001 (2013)
6. R. Aaij et al. (LHCb), Phys. Rev. Lett. **115**, 072001 (2015)
7. C. Adolph et al. (COMPASS), Phys. Rev. Lett. **115**(8), 082001 (2015)
8. R. Aaij et al. (LHCb), Phys. Rev. Lett. **122**(22), 222001 (2019)
9. R. Aaij et al. (LHCb), Sci. Bull. **66**, 1278–1287 (2021)
10. (LHCb), arXiv:2210.10346 [hep-ex]
11. M. Gell-Mann, Phys. Lett. **8**, 214–215 (1964)
12. J.J. Wu, R. Molina, E. Oset, B.S. Zou, Phys. Rev. Lett. **105**, 232001 (2010)
13. J.J. Wu, R. Molina, E. Oset, B.S. Zou, Phys. Rev. C **84**, 015202 (2011)
14. H.X. Chen, W. Chen, X. Liu, S.L. Zhu, Phys. Rep. **639**, 1–121 (2016)
15. F.K. Guo, C. Hanhart, U.-G. Meißner, Q. Wang, Q. Zhao, B.S. Zou, Rev. Mod. Phys. **90**(1), 015004 (2018) [erratum: Rev. Mod. Phys. **94** (2022) no.2, 029901]
16. Y.R. Liu, H.X. Chen, W. Chen, X. Liu, S.L. Zhu, Prog. Part. Nucl. Phys. **107**, 237–320 (2019)
17. N. Brambilla, S. Eidelman, C. Hanhart, A. Nefediev, C.P. Shen, C.E. Thomas, A. Vairo, C.Z. Yuan, Phys. Rep. **873**, 1–154 (2020)
18. L. Meng, B. Wang, G.J. Wang, S.L. Zhu, arXiv:2204.08716 [hep-ph]
19. X.K. Dong, F.K. Guo, B.S. Zou, Phys. Rev. Lett. **126**(15), 152001 (2021)
20. M.Z. Liu, J.J. Xie, L.S. Geng, Phys. Rev. D **102**(9), 091502 (2020)
21. K. Chen, B. Wang, S.L. Zhu, Phys. Rev. D **103**(11), 116017 (2021)
22. X.K. Dong, F.K. Guo, B.S. Zou, Commun. Theor. Phys. **73**(12), 125201 (2021)
23. R. Chen, N. Li, Z.F. Sun, X. Liu, S.L. Zhu, Phys. Lett. B **822**, 136693 (2021)
24. X.K. Dong, F.K. Guo, B.S. Zou, Progr. Phys. **41**, 65–93 (2021)
25. C.W. Shen, U.-G. Meißner, Phys. Lett. B **831**, 137197 (2022)
26. D. Gülmez, U.-G. Meißner, J.A. Oller, Eur. Phys. J. C **77**(7), 460 (2017)
27. M.L. Du, D. Gülmez, F.K. Guo, U.-G. Meißner, Q. Wang, Eur. Phys. J. C **78**(12), 988 (2018)
28. S. Weinberg, Phys. A **96**(1–2), 327–340 (1979)
29. J. Gasser, H. Leutwyler, Ann. Phys. **158**, 142 (1984)
30. J. Gasser, H. Leutwyler, Nucl. Phys. B **250**, 465–516 (1985)
31. V. Bernard, U.-G. Meißner, Annu. Rev. Nucl. Part. Sci. **57**, 33–60 (2007)
32. M.B. Wise, Phys. Rev. D **45**(7), R2188 (1992)
33. T.M. Yan, H.Y. Cheng, C.Y. Cheung, G.L. Lin, Y.C. Lin, H.L. Yu, Phys. Rev. D **46**, 1148–1164 (1992) [erratum: Phys. Rev. D **55** (1997), 5851]
34. H.Y. Cheng, C.Y. Cheung, G.L. Lin, Y.C. Lin, T.M. Yan, H.L. Yu, Phys. Rev. D **47**, 1030–1042 (1993)
35. R. Casalbuoni, A. Deandrea, N. Di Bartolomeo, R. Gatto, F. Feruglio, G. Nardulli, Phys. Rep. **281**, 145–238 (1997)
36. M. Bando, T. Kugo, S. Uehara, K. Yamawaki, T. Yanagida, Phys. Rev. Lett. **54**, 1215 (1985)
37. M. Bando, T. Kugo, K. Yamawaki, Phys. Rep. **164**, 217–314 (1988)
38. U.-G. Meißner, Phys. Rep. **161**, 213 (1988)
39. Y.R. Liu, M. Oka, Phys. Rev. D **85**, 014015 (2012)
40. J. Nieves, M.P. Valderrama, Phys. Rev. D **86**, 056004 (2012)
41. J.A. Oller, E. Oset, J.R. Pelaez, Phys. Rev. D **59**, 074001 (1999) [erratum: Phys. Rev. D **60** (1999), 099906; erratum: Phys. Rev. D **75** (2007), 099903]
42. J.A. Oller, E. Oset, J.R. Pelaez, Phys. Rev. Lett. **80**, 3452–3455 (1998)
43. J.A. Oller, E. Oset, Phys. Rev. D **60**, 074023 (1999)
44. J.A. Oller, E. Oset, Nucl. Phys. A **620**, 438–456 (1997) [erratum: Nucl. Phys. A **652** (1999), 407–409]
45. J.A. Oller, U.-G. Meißner, Phys. Lett. B **500**, 263–272 (2001)
46. M.F.M. Lutz, E.E. Kolomeitsev, Nucl. Phys. A **700**, 193–308 (2002)
47. C. Garcia-Recio, J. Nieves, E. Ruiz Arriola, M.J. Vicente Vacas, Phys. Rev. D **67**, 076009 (2003)
48. D. Jido, J.A. Oller, E. Oset, A. Ramos, U.-G. Meißner, Nucl. Phys. A **725**, 181–200 (2003)
49. T. Hyodo, W. Weise, Phys. Rev. C **77**, 035204 (2008)
50. Z.H. Guo, J.A. Oller, J. Ruiz de Elvira, Phys. Rev. D **86**, 054006 (2012)
51. M. Albaladejo, P. Fernandez-Soler, F.K. Guo, J. Nieves, Phys. Lett. B **767**, 465–469 (2017)
52. M.L. Du, F.K. Guo, U.-G. Meißner, D.L. Yao, Eur. Phys. J. C **77**(11), 728 (2017)

53. G.F. Chew, S. Mandelstam, Phys. Rev. **119**, 467–477 (1960)
54. J.D. Bjorken, Phys. Rev. Lett. **4**, 473–474 (1960)
55. L. Castillejo, R.H. Dalitz, F.J. Dyson, Phys. Rev. **101**, 453–458 (1956)
56. C. Isola, M. Ladisa, G. Nardulli, P. Santorelli, Phys. Rev. D **68**, 114001 (2003)
57. N. Yalikun, Y.H. Lin, F.K. Guo, Y. Kamiya, B.S. Zou, Phys. Rev. D **104**(9), 094039 (2021)
58. R. Chen, F.L. Wang, A. Hosaka, X. Liu, Phys. Rev. D **97**(11), 114011 (2018)
59. Z.L. Wang, C.W. Shen, D. Rönchen, U.-G. Meißner, B.S. Zou, Eur. Phys. J. C **82**(5), 497 (2022)
60. Z.L. Wang, B.S. Zou, Eur. Phys. J. C **82**(6), 509 (2022)